Eur. Phys. J. Special Topics **224**, 3199–3210 (2015)

DOI: 10.1140/epjst/e2015-50078-x

THE EUROPEAN PHYSICAL JOURNAL SPECIAL TOPICS

Regular Article

Paramecia swimming in viscous flow

P. Zhang[1], S. Jana[1], M. Giarra[2], P.P. Vlachos[2,3], and S. Jung[1,a]

[1] Department of Engineering Science and Mechanics, Virginia Tech, Blacksburg, VA 24061, USA
[2] Department of Mechanical Engineering, Virginia Tech, Blacksburg, VA 24061, USA
[3] School of Mechanical Engineering, Purdue University, West Lafayette, IN 47907, USA

Received 30 March 2015 / Received in final form 2 November 2015
Published online 15 December 2015

Abstract. Ciliates like *Paramecia* exhibit fore-aft asymmetry in their body shapes, and preferentially swim in the direction of the slender anterior rather than the wider posterior. However, the physical reasons for this preference are not well understood. In this work, we propose that specific features of the fluid flow around swimming *Paramecia* confer some energetic advantage to the preferred swimming direction. Therefore, we seek to understand the effects of body asymmetry and swimming direction on the efficiency of swimming and the flux of fluid into the cilia layer (and thus of food into the oral groove), which we assumed to be primary factors in the energy budgets of these organisms. To this end, we combined numerical techniques (the boundary element method) and laboratory experiments (micro particle image velocimetry) to develop a quantitative model of the flow around a *Paramecium* and investigate the effect of the body shape on the velocity fields, as well as on the swimming and feeding behaviors. Both simulation and experimental results show that velocity fields exhibit fore-aft asymmetry. Moreover, the shape asymmetry revealed an increase of the fluid flux into the cilia layer compared to symmetric body shapes. Under the assumption that cilia fluid intake and feeding efficiency are primary factors in the energy budgets of *Paramecia*, our model predicts that the anterior swimming direction is energetically favorable to the posterior swimming direction.

1 Introduction

Many micro-organisms swim in viscous environments to seek nutrients [1] or escape from predators [2,3]. In the highly resistive environments, both swimming and nutrient intake might be adjusted to be hydrodynamically efficient [4,5]. Micro-organisms swim as a result of fluid flows around the body created by propulsive organelles (e.g. flagellum, cilium, etc.) [6,7]. Simultaneously, nutrients are advected into the oral grooves by the fluid flow for large ciliates, or diffused across cell membranes by Brownian motion for small bacteria or eukaryotes [8,9]. Both swimming and feeding are thus governed by flow fields generated by active organelles [10].

[a] e-mail: sunnyjsh@vt.edu

Paramecium has been used as a model system to understand the biology of ciliates [11]. The swimming and food-intake behaviors of *Paramecium* are governed by the ciliary motion on the body surface [12]. While experimental investigations into flows around *Chlamydomonas* [13] and bacteria [14] has gained momentum, studies involving flow-field around unicellular ciliates remain extremely rare. Ciliary organisms present a unique complexity in terms of the multitude of ciliary hairs all over the cell body, which may be beating differently under varying stimuli leading to complicated flow-fields. Until recently, there have been only a few investigative attempts to quantify the flows created by ciliates. Keller and Wu [15] photographed streaklines around *Paramecium* which qualitatively supported their theoretical model. Recently, Kim et al. measured the magnitudes of velocity around a turning *Tetrahymena* at a low spatial resolution [16].

The body of a *Parameicum* is roughly in the shape of a prolate spheroid [15]; more precisely it has a slender anterior and a bulky posterior. In the natural environment, *Paramecia* swim at about 1.5 mm/s in a helical path along the anterior [17], which is their preferred swimming direction. While swimming, *Paramecia* ingest bacteria or other nutrients contained in the fluid. The fluid containing nutrients is first swept into the cilia layer, and then pushed into the oral groove which is located in the middle of the cell body and has an opening towards the anterior [11].

Despite the shapes of *Paramecia* and many other ciliates being fore-aft asymmetric, previous theoretical and computational models have focused on symmetric shapes [18–20] or on deformed shapes due to the metachronal wave [21]. Blake [18] modeled swimming of ciliates as spheres with shear surface velocity. Further, Keller and Wu [15] modeled *Paramecia* as prolate spheroids and analytically calculated swimming velocity and energy dissipation for different surface velocities. Recently, an optimal symmetric *Paramecium* body shape that minimize the total power output was numerically obtained [22]. The analytical or numerical investigations have thus been limited to fore-aft symmetric body with surface velocities [19], which are not representative of many ciliates including *Paramecia*.

The boundary element method has been widely used to model moving objects in a viscous fluid [20,23]. Once topological shapes and boundary conditions are determined, the pressure and velocity distribution in the fluid can be obtained through boundary integral representations. Such numerical studies allow us to calculate the surface force and velocity, and further evaluate the power of the swimming organism [23]. Most previous simulations have assumed only shear velocity over an ellipsoid body surface as boundary conditions [18–20]. However, if the fluid motion in the cilia layer is considered, the net fluid flux should be zero due to the incompressibility of the fluid. Therefore, for a certain distribution of shear velocity, normal surface velocity should exist in order to satisfy this zero-flux condition in the cilia layer. Such boundary conditions have originally been introduced by Keller & Wu [15], however, not much work has followed and it has not been generalized to asymmetric shapes.

Both *Paramecia*'s body shapes and surface velocities are attributed to surrounding fluid flows. However, surface velocity varies significantly among different *Paramecia*, therefore, our current study will focus on the hydrodynamic effect of body shape. In this paper, we investigate the swimming and feeding behaviors of *Paramecia* by considering their fore-aft asymmetric body shapes and fluid volume conservation in the cilia layer. Experimentally, micro particle image velocimetry (μ-PIV) is employed to resolve the velocity field. For simulations, the boundary element method is employed to simulate the flow field around the asymmetric bodies with both normal and shear surface velocities satisfying volume conservation in the cilia layer. Finally, swimming efficiency and feeding velocity are examined to gain insight into the effect of body shapes and swimming direction. Under the assumption that cilia fluid intake and feeding efficiency are primary factors in the energy budgets of *Paramecia*, this study

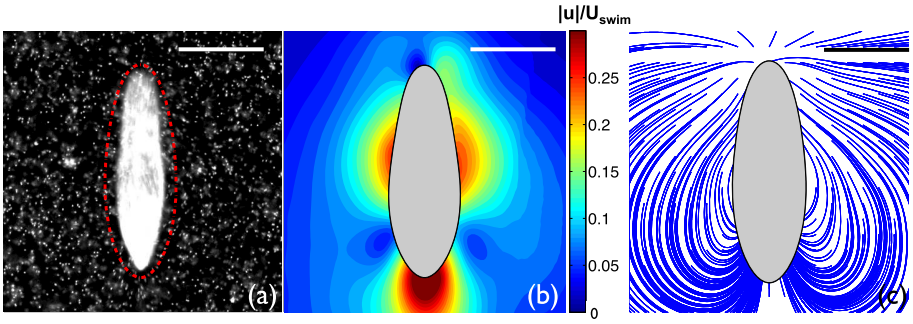

Fig. 1. (a) Dark-field image of a *Paramecium* swimming in a suspension of polystyrene spheres. (Supplementary Movie 1). The red dotted lines represents the cilia layer of constant thickness around the cell body. (b) Velocity magnitudes around the *Paramecium* averaged over different frames (Supplementary Movie 2). (c) Integrated pathlines from the average velocities around the *Paramecium*. All scale bars are 100 μm.

predicts that the anterior swimming direction is favorable to the posterior swimming direction.

2 Experimental methods

2.1 Culturing methods

Paramecium multimicronucleatum originally obtained from Carolina Biological Supply was cultured using double wheat medium in spring water [25]. Cells were harvested during 8–11 day of their culture, which corresponds to their growth phase and were washed twice in Tris HCl buffer solution [17]. Separately, 1 ml of an aqueous suspension of red fluorescent polystyrene microspheres (2% by volume; Thermo Scientific) were centrifuged at 7200 g and the supernatant (containing the stabilizing surfactant solution) was decanted (as the surfactant caused cell death). About 5.5 μl of the residual polystyrene spheres were pipetted into 1.1 ml of the freely swimming *Paramecia* culture. The suspension (particle concentration $\approx$0.5%) was shaken gently to ensure uniform distribution of the particles in the fluid media.

2.2 Particle image velocimetry methods

The suspension of *Paramecia* and particles was put on a glass slide. Two plastic spacers of 754 μm thickness were used to create a fluid film of uniform thickness sandwiched between two glass slides. Controlling the thickness parameter was important because it was previously observed that nearby boundaries tend to change the motility mode of *Paramecia*. The semi-major axis of *Paramecia* in the trials were 117 ± 6 μm (one standard deviation) and the semi-minor axis was found to be 38 ± 2 μm in length. The sample was placed on the stage of a Leica DMI 3000B microscope and an array of LED lights (LED-12 from IDT in continuous mode) was used for illumination. Since the LED array was placed at an oblique angle, it allowed us to obtain very high contrast dark field type images that showed bright white particles and *Paramecia* on a black background (as shown in Fig. 1(a)). The motions of *Paramecia* were recorded at 100 frames per second with a 15$\times$ microscope objective lens and a high speed camera (MotionXtra N3 from IDT) with 1280$\times$1024 pixels, which resulted in an image magnification of 0.725 μm/pixel.

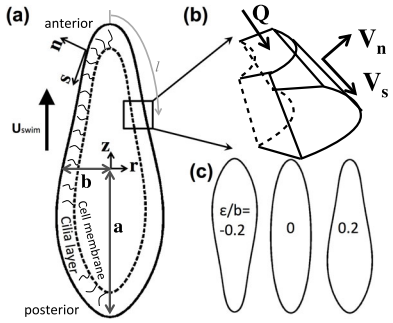

Fig. 2. (a) Illustration of *Paramecium* body shape with cilia layer and (b) control volume on cilia layer. (c) Body shapes defined by Eq. (1) with parameters $e = 0.944$ for $\epsilon/b = -0.2, 0$ and 0.2.

The acquired images were processed using the Prana PIV code [26–28] with a multigrid multiframe discrete window offset technique [29,30] with an interrogation window size of 64×64 pixels and 82.5% overlap between the interrogation regions. *Paramecia* were free to swim along any direction and hence their orientations were different in the movies recorded. We defined an inertial coordinate frame (moving frame) attached to the center of the body of the organism. After aligning the different orientations of the *Paramecium* along each specified frame we calculate the time averaged velocity field over a sequence of frames. In the experiments, we only considered the cases in which the *Paramecia* were freely swimming in a straight line and the rotational motions were neglected. As a representative result, Fig. 1(b) shows the averaged velocity and integrated pathlines (Fig. 1(c)) around the body of a swimming *Paramecium*. One can observe that there is a fore-aft asymmetry of the pathlines in Fig. 1, while the symmetry about the axial direction is still maintained.

2.3 Body shapes

Paramecium body shapes can be approximated by prolate spheroids with small variations. Denoting the radial position of the outer cilia layer as R and longitudinal position as z, then the radial position can be written as,

$$R(z) = b\left[(1 - z^2/a^2)^{1/2} - \frac{\epsilon}{b}\sin(\pi z/a)\right], \tag{1}$$

where a and b are lengths of semi-major and semi-minor axes (Fig. 2(a)). By varying the asymmetry parameter ϵ/b, different body shapes can be obtained and are shown in Fig. 2(c).

In experiments we found that *Paramecia* are bulkier at the posterior end. In order to quantify this fore-aft asymmetry, we used Eq. (1) and measured the parameter ϵ/b. Major and minor axes lengths of real *Paramecia* shapes defined in Eq. (1) were measured to give an eccentricity value. Body asymmetry (ϵ/b) was then measured by finding the best fitting curve using Eq. (1) for the observed shapes.

3 Numerical methods

The boundary element method is used to simulate swimming of *Paramecium* with body shapes defined by Eq. (1). The accuracy of the simulation will be verified against

theoretical results on swimming spheroids [15]. The numerical results will be combined with the measured surface velocities from the experiments and the results will be shown in Sect. 5.

In experiments, we observed that *Paramecia* swim at a speed of about 1.5 mm/s in fluid media of 1 mPa·s viscosity. The corresponding Reynolds number (a ratio of fluid inertia to viscous effects) is about 0.2, which belongs to the low Reynolds number regime. The motion of surrounding fluid around *Paramecia* is therefore assumed to be governed by the Stokes equations,

$$-\nabla p + \mu \nabla^2 \boldsymbol{u} = 0, \nabla \cdot \boldsymbol{u} = 0, \tag{2}$$

where $\boldsymbol{u}$ is the fluid velocity, p is the pressure and μ the dynamic viscosity. For a freely moving body (denoted by D) with no acceleration, the total hydrodynamic force ($\boldsymbol{F}$) and torque ($\boldsymbol{L}$) on the body are equal to zero, which can be written as,

$$\boldsymbol{F} = \int_{\partial D} \boldsymbol{f}\, dS = \boldsymbol{0}, \boldsymbol{L} = \int_{\partial D} \boldsymbol{x} \times \boldsymbol{f}\, dS = \boldsymbol{0}, \tag{3}$$

where $\boldsymbol{f}$ is the surface force at a point $\boldsymbol{x}$ on the body surface (∂D).

In the present work, the boundary element method was used to simulate the flow around the swimming *Paramecium*. The velocity at point $\boldsymbol{x_0}$ in the fluid can be computed by the boundary element formulation in three dimensions, with known surface velocity and force [23,31], as,

$$\boldsymbol{u}(\boldsymbol{x}_0) = -\frac{1}{8\pi\mu} \int_{\partial D} \boldsymbol{U}(\boldsymbol{x_0}, \boldsymbol{x}) \boldsymbol{f}(\boldsymbol{x})\, dS(\boldsymbol{x}), \tag{4}$$

where Stokeslet $\boldsymbol{U}(\boldsymbol{x},\boldsymbol{y})$ is defined as,

$$U_{ij}(\boldsymbol{x}, \boldsymbol{y}) = \frac{\delta_{ij}}{r} + \frac{(x_i - y_i)(x_j - y_j)}{r^3}, \tag{5}$$

with $r = |\boldsymbol{x} - \boldsymbol{y}|$. The integrals in Eq. (4) can be evaluated numerically based on the discretization of the surface, which gives the linear system,

$$\boldsymbol{u} = \boldsymbol{A}\boldsymbol{f}, \tag{6}$$

where vectors $\boldsymbol{u}$ and $\boldsymbol{f}$ contain velocity and force values at collocation points and $\boldsymbol{A}$ is the influence matrix.

The outer surface of the cilia layer was discretized into $N = 512$ curved triangular elements, with the collocation points $\boldsymbol{x_0}$ located at the center of the triangle. Triangulation of the body surface and numerical integration of Eq. (4) in the simulation were performed by a program developed by Pozrikidis [32]. All linear systems were solved by LU decomposition algorithms in this paper.

Paramecia beat their cilia in certain ways to create surface velocity, which results in the translation and rotation of the body in a viscous fluid. In our study, only translational motion along the $\boldsymbol{e_z}$ direction was considered. Values of translational velocity U_{swim} can be generated by different surface velocities, so the resulting surface velocity in the laboratory frame can be expressed as,

$$\boldsymbol{u}(\boldsymbol{x_c}) = \boldsymbol{u_s}(\boldsymbol{x_c}) + U_{\text{swim}} \boldsymbol{e_z}, \tag{7}$$

where $\boldsymbol{u_s}$ is the surface velocity in the moving frame, which has components in both normal ($\boldsymbol{n}$) and shear ($\boldsymbol{s}$) directions as,

$$\boldsymbol{u_s}(\boldsymbol{x}) = V_n(\boldsymbol{x})\boldsymbol{n} + V_s(\boldsymbol{x})\boldsymbol{s}\,. \tag{8}$$

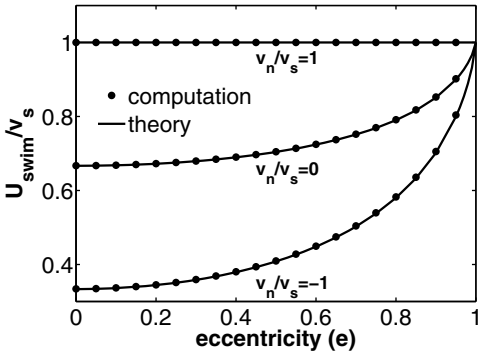

Fig. 3. Swimming velocities for ellipsoid body shapes. Surface velocity is defined in Eq. (9) with different v_n/v_s values.

Velocities generated by cilia on the outer cilia layer have been modeled in [15] as,

$$V_n(\boldsymbol{x}) = -v_n \boldsymbol{n}(\boldsymbol{x}) \cdot \boldsymbol{e_z}, V_s(\boldsymbol{x}) = -v_s \boldsymbol{s}(\boldsymbol{x}) \cdot \boldsymbol{e_z}. \tag{9}$$

To validate the accuracy of the proposed computational scheme, swimming velocities of ellipsoids given by the boundary element method are compared with theoretical results for different eccentricities [15] as shown in Fig. 3.

4 A simplified model

As shown in Fig. 1, the flow patterns and velocity magnitude distribution do not preserve fore-aft symmetry. This asymmetry in the flow field is likely the consequence of two asymmetries in boundary conditions. One noticeable asymmetry in boundary conditions is the distribution of surface normal and shear velocities. As will be shown in Fig. 4(b) Sect. 5.2, V_s and V_n are not symmetric about the equatorial plane ($z = 0$). For all cases measured in experiments, shear velocities V_s are larger at the anterior than at the posterior. The other asymmetry comes from the body shapes of *Paramecia*, as discussed in Sect. 2.3. The body shape asymmetry has been parameterized by a single value ϵ/b. The asymmetry of surface velocity, however, is difficult to parameterize due to the complexity and randomness of variations among different cases. Therefore, the current work focuses on modeling the asymmetry of velocity fields around swimming *Paramecia* as a consequence of asymmetric body shapes.

To better reflect real swimming conditions, $V_n(\boldsymbol{x})$ and $V_s(\boldsymbol{x})$ in the simulation are defined to satisfy fluid volume conservation in cilia layers. It has been observed that the cilia layer covers the *Paramecium* body uniformly and beats at the same frequency. To model such physical shear velocity around the body, V_s is chosen as proposed by Keller & Wu [15]. Further, we assume the shear flow field in the cilia layer has a half-parabolic distribution: $\boldsymbol{u} \cdot \boldsymbol{s} = V_s\,(2L_{\text{cilia}} - y)y$, where L_{cilia} is the thickness of cilia layer; y is the coordinate along the normal direction to the cell body. This assumption of a half-parabolic profile is justified by comparing with measured surface velocities and surrounding pathlines, as will be discussed in Fig. 4(b) and Fig. 6. Normal velocity was then determined by conservation of fluid volume in the cilia layer. With varying radial position $R(z)$, a non-zero normal velocity can be determined by

confining the total flux into the control volume to be zero,

$$V_s(\boldsymbol{x}) = -v_s \boldsymbol{s}(\boldsymbol{x})|_{\text{ellipsoid}} \cdot \boldsymbol{e_z} \,,$$

$$V_n(\boldsymbol{x}) = \frac{1}{2\pi R} \frac{dQ(l(\boldsymbol{x}))}{dl}, \tag{10}$$

where $\boldsymbol{s}(\boldsymbol{x})|_{\text{ellipsoid}}$ is the shear velocity at the surface $\boldsymbol{x}$ on the non-deformed ellipsoid with the same eccentricity from [15]; $l(\boldsymbol{x})$ is a parametric arc length coordinate measured from $z = a$ to $z = -a$ along the outer cilia layer (Fig. 2(a)); $Q(l)$ is the fluid flux through the intersection of the cilia layer (Fig. 2(b)). For a spherical body with radius R_0, V_n becomes $V_n(z) = v_s z(4/3 - L_{\text{cilia}}/2R_0)L_{\text{cilia}}/R_0^2$. Once the surface velocity was known, Eq. (4) could produce velocity at any point in the fluid from which the pathlines around the *Paramecium* body were integrated. Note that the velocities in Eq. (10) are applied on the outer cilia layer.

The asymmetric body shapes may lead to changes in the swimming and feeding behaviors. To obtain a quantitative evaluation of the efficiency, we first define the energy dissipation of a swimming *Paramecium* by

$$P = \int_{\partial D} \boldsymbol{f} \cdot \boldsymbol{v} \, dS + \int_{D_{\text{cilia layer}}} \mu |\nabla \boldsymbol{u}|^2 d\text{V}, \tag{11}$$

where the first term represents the energy dissipation outside the cilia layer and the second is the energy dissipation inside the cilia layer. We then use the classic definition of the swimming efficiency,

$$\eta_{\text{swim}} = \frac{\mu |U_{\text{swim}}|^2 a}{P}, \tag{12}$$

where a is the semi-major axis of the swimming body. In the present study, we keep a fixed for all simulations and focus on the effect of different ϵ/b values.

Since the oral groove of a *Paramecium* is located at the center of the body and has an opening pointing towards the anterior, the fluid entering the anterior half of the cilia layer has the possibility of entering the oral groove. Therefore, considering the possibility of the fluid being fed, we define the feeding velocity as the fluid flux into the anterior half of the cilia layer averaged by the corresponding surface area,

$$U_{\text{feed}} = \frac{\int_{\partial D_{(z>0)}} -\boldsymbol{u_s}(\boldsymbol{x}) \cdot \hat{\boldsymbol{n}} dS}{\int_{\partial D_{(z>0)}} dS}, \tag{13}$$

where $\partial D_{(z>0)}$ denotes anterior half of the cilia layer surface. Similar to the swimming efficiency, we define the feeding efficiency as,

$$\eta_{\text{feed}} = \frac{\mu |U_{\text{feed}}|^2 a}{P}. \tag{14}$$

5 Results

In this section, we experimentally measure *Paramecia*'s body shapes, surface velocity and surrounding velocity field. Calculated pathlines and velocity magnitude are compared with simulation results using measured surface velocity as input boundary conditions. The effect of body shape on the velocity field is studied by simulations using modeled surface velocities as boundary conditions. In addition, velocity decay rates in the far field are also measured and compared with simulation results. From the simulations, swimming and feeding efficiencies are calculated on different body shapes.

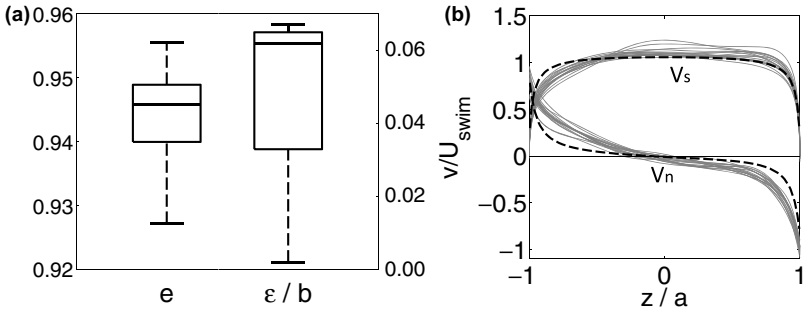

Fig. 4. (a) Box plot of measured eccentricity e and ϵ/b values from sixteen different *Paramecia*. (b) Comparison of normal and shear surface velocities in moving frame for sixteen cases. Velocities (thin solid lines) in (b) are measured from experiments. Modeled surface velocities are shown in thick dotted lines ($e = 0.944, \epsilon/b = 0.05$).

5.1 Body shape

The eccentricity and asymmetry parameter of real *Paramecia* are measured from 16 different organisms. The eccentricity value ($e = \sqrt{1 - b^2/a^2}$) was measured to be $e = 0.944 \pm 0.007$. The asymmetry parameter ϵ/b defined in Eq. (1) was determined to be 0.048 ± 0.022. Statistics of e and ϵ/b values are shown in Fig. 4(a). Large e values indicate that the body lengths of *Paramecia* are much larger than body widths. Positive ϵ/b values result from the fact that *Paramecia* swim towards the slender anterior. For the 16 cases measured in the experiment, ϵ/b values are all positive.

We hypothesize that the bulkier posterior is one of the reasons that lead to the asymmetric pathlines, as asymmetric fluid boundary shape causes asymmetric flow field. In order to understand such geometric effects on the swimming and feeding performances, we used boundary element method to model the flow around the swimmers.

5.2 Measured velocity field

Measured surface velocities $V_n(\boldsymbol{x})$ and $V_s(\boldsymbol{x})$ are compared with modeled surface velocities given by Eq. (10) for $\epsilon/b = 0.048$ in Fig. 4(b). Pathlines and velocity magnitudes of three different cases are shown on the top row of Fig. 5. Measured surface velocities are then used as boundary conditions in simulations and the resulting pathlines and velocity magnitude are shown on the bottom row of Fig. 5.

Good agreement between experiments and simulation results has been observed in terms of overall shapes of pathlines and velocity magnitude. Some discrepancies are also found in velocity magnitude distributions. Measured velocity magnitude appears to be greater than numerical results. There are two possible sources of errors. First, the rotational motions of *Paramecia* were not incorporated in simulations. In experiments, *Paramecia* rotated around their major axis and this rotation combined with a small yaw caused the centers of the bodies to move in helical paths. We observed that the rotation speed was approximately a half of the translational speed, which indicates that the horizontal flow motions were dominant. Therefore, we did not include rotation in our simulations. Second, in our experiments the *Paramecia* suspension was deposited between two parallel plates, which could have wall effects on the *Paramecia* motion. The presence of walls may also lead to a larger velocity magnitude.

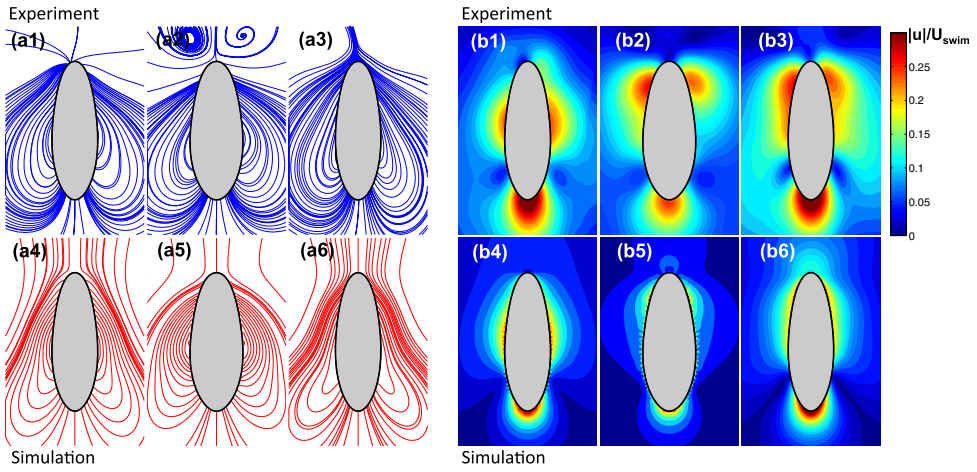

Fig. 5. Comparison of (a) pathlines and (b) velocity magnitude from experiments (top row) and simulation results using experimentally measured surface velocities (bottom row). Pathlines (a 1-6) correspond to velocity magnitude (b 1-6). Eccentricity $e = 0.949, 0.937, 0.951$ and deformation parameter $\epsilon/b = 0.062, 0.064, 0.065$ for body shapes (a 1-3), respectively. All results are shown in lab frame.

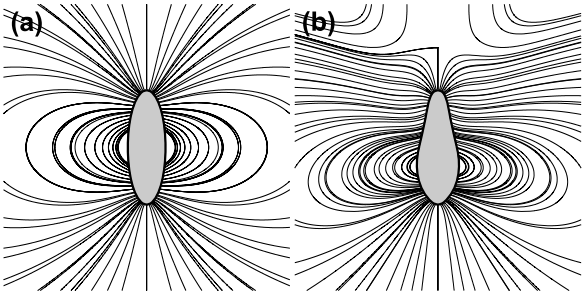

Fig. 6. Velocity pathlines around the swimming body using modeled surface velocities for $e = 0.944$, (a) $\epsilon/b = 0$ and (b) $\epsilon/b = 0.2$.

5.3 Simulated velocity field

As shown in Fig. 4(b), surface velocities modeled by (10) can follow the general distributions of measured values. However, modeled velocities cannot capture the local asymmetries or randomness among different cases. For example, in some cases higher V_s were observed near the anterior than the posterior. Therefore, current work focuses on the effect of body shape asymmetry rather than surface velocity asymmetry.

Simulated pathline patterns using modeled surface velocity for $\epsilon/b = 0$ and $\epsilon/b = 0.2$ are shown in Fig. 6. In order to show the effect of body shape, the asymmetry parameter is chosen to be $\epsilon/b = 0.2$, which is larger than measured asymmetry in experiments. It is found that for ellipsoid body shape ($\epsilon/b = 0$), pathlines around the moving body exhibit fore-aft symmetry, as expected in a viscous fluid. For slender anterior body shapes ($\epsilon/b > 0$), velocity pathlines have asymmetric shapes that bend towards the posterior of the body similar to experimental observations.

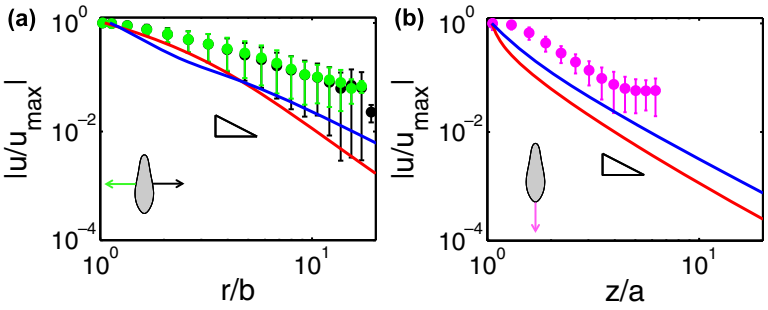

Fig. 7. Comparisons of normalized velocity magnitude distribution along equatorial and axial directions between experiment and simulation. Decay of velocity in experiment along three directions are indicated by three colors (green, black and magenta) shown in the insets, with uncertainty bars indicating standard deviation of 16 measurements. Measured velocities (a) on the equatorial plane and (b) along posterior direction are compared with simulation results. Simulation results given by proposed surface velocity (in red) and experimentally measured surface velocity (in blue) are shown in each sub-figure with corresponding directions of velocity distributions. A slope of -2 is shown by a triangle in each sub-figure.

The experimentally measured velocity decay along directions parallel and perpendicular to the swimming direction are also compared with simulation results in Fig. 7. For velocity along equatorial plane as shown in Fig. 7(a), both measured and simulated velocities decay approximately as r^{-2}. The large uncertainty in the velocity along equatorial plane might be introduced by the 3D rotational motion of the *Paramecium*, which causes the body to move in and out of the focal plane. Velocity measurements along the posterior direction is more accurate because the posterior was observed to always remains in the focal plane. Along the posterior direction, we found that the decay rate ($\sim r^{-2}$) of velocity magnitude agrees well with simulation results.

When a fore-aft symmetric body moves in a viscous fluid, the anterior and posterior halves of the body experience an equal amount of drag and propulsion, the total effect of which in the far field is a source dipole that decays as r^{-3}. However, for an asymmetric *Paramecium* body, the anterior half experiences a net drag and the posterior half a net propulsive force, which induces a force separation. This force separation from the equatorial plane has the effect of a force dipole that decays as r^{-2}, which is close to our experiment data. It is also worth mentioning that the force dipole induced by the body fore-aft asymmetry can produce a flow field similar to that of a pusher squirmer [33].

5.4 Effect of body shapes on swimming and feeding

The variation in efficiencies as a function of asymmetry parameter (ϵ/b) are shown in Fig. 8. Figure 8(a) shows that any asymmetry in the body shape decreases the swimming efficiency. However, a body swimming to the slender anterior has higher feeding efficiency (Fig. 8(b)) and more fluid intake (Fig. 8(c,d)), as a result of more fluid flux into the cilia layer on the anterior part. These computational calculations of efficiencies and fluid flux indicate that when *Paramecia* swim towards the slender anterior, they are able to achieve more food intake with certain loss of swimming efficiency.

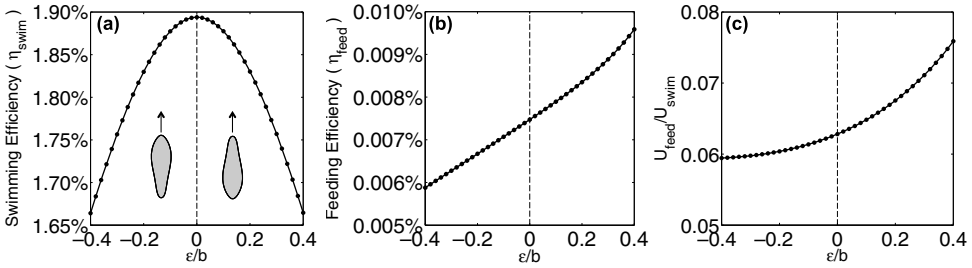

Fig. 8. (a) Swimming efficiency; (b) feeding efficiency; (c) feeding velocity normalized by U_{swim}. Eccentricity $e = 0.944$ is used in all simulations.

6 Conclusions

We investigated the swimming and feeding of fore-aft asymmetric *Paramecia*. The asymmetric velocity pathline patterns were observed experimentally by μ-PIV and were re-constructed numerically. The boundary element method was used in simulations on asymmetric body shapes with normal and shear velocities given by the proposed model. Asymmetry of body shapes and distribution of surface velocity are believed to account for the fore-aft asymmetric flow field around the swimming body. The body shape of *Paramecium* was parameterized to study its effect on velocity field around the body. The effect of body asymmetry on swimming and feeding behaviors was also studied.

Based on our model, body shapes with large asymmetry parameters created obvious asymmetries in velocity pathlines, which were qualitatively similar to experiment observations. However, due to the small ϵ/b values measured experimentally, we believe that the asymmetry in surface velocities was another significant factor that led to asymmetric flow field, which we did not explore in details in current work. We found that the swimming efficiencies for anterior and posterior swimming directions were equivalent for a given degree of body asymmetry. Therefore, under the assumption that cilia fluid intake and feeding efficiency are primary factors in the energy budgets of *Paramecia*, our model predicted that the anterior swimming direction was favorable to the posterior swimming direction.

Several possible sources of errors existed in our experiments. Rotational motion of *Paramecium* was neglected in proposed model due to the difficulty in validating the rotational surface velocity. However, the rotation of *Paramecium* body may lead to an increased velocity magnitude around the body. The fact that *Paramecia* were confined between two parallel plates in experiment had a similar effect. Small ambient flow could also cause error in velocity measurements in the far field.

For future work, a modified model that incorporates the rotational and helical motion of *Paramecium* may help better understand the swimming mechanisms. Asymmetry in surface velocities should also be considered as an important factor to account for the asymmetric flow. Moreover, the authors are also aware that not all fluid entering the cilia layer of the anterior half of the body can be fed by *Paramecia*. The definition of feeding velocity can be modified and will be more helpful if further studies can be done on *Paramecia* feeding behavior [34].

This research was partially supported by National Science Foundation (PHY-1205642, CBET-1336038) and the Virginia Tech Institute for Critical Technology and Applied Science.

References

1. T. Fenchel, Sci. **296**, 1068 (2002)
2. J. Sheng, E. Malkiel, J. Katz, J. Adolf, R. Belas, A.R. Place, Proc. Natl. Acad. Sci. USA **104**, 17512 (2007)
3. E. Lauga, T.R. Powers, Rep. Prog. Phys. **72**, 096601 (2009)
4. S. Michelin, E. Lauga, Phys. Fluids **23**, 101901 (2011)
5. D. Tam, A.E. Hosoi, Proc. Natl. Acad. Sci. USA **108**, 1001 (2011)
6. J.O. Kessler, Nature **313**, 218 (1985)
7. J.S. Guasto, K.A. Johnson, J.P. Gollub, Phys. Rev. Lett. **105**, 168102 (2010)
8. V. Magar, T.J. Pedley, J. Fluid Mech. **539**, 93 (2005)
9. J.S. Guasto, R. Rusconi, R. Stocker, Ann. Rev. Fluid Mech. **44**, 373 (2012)
10. C. Brennen, H. Winet, Ann. Rev. Fluid Mech. **9**, 339 (1977)
11. R. Wichterman, *The biology of Paramecium* (Plenum Press, New York/London, 1986)
12. H. Machemer, J. Exp. Biol. **57**, 239 (1972)
13. K. Drescher, R.E. Goldstein, N. Michel, M. Polin, I. Tuval, Phys. Rev. Lett. **105**, 168101 (2010)
14. K. Drescher, J. Dunkel, L.H. Cisneros, S. Ganguly, R.E. Goldstein, Proc. Natl. Acad. Sci. USA **108**, 10940 (2011)
15. S.R. Keller, T.Y. Wu, J. Fluid Mech. **80**, 259 (1977)
16. J. Kim, Y. Jang, D. Byun, M. Kim, S.W. Nam, S. Park, J. Vis. **14**(4), 361 (2011)
17. S. Jana, S.H. Um, S. Jung, Phys. Fluids **24**, 041901 (2012)
18. J.R. Blake, J. Fluid Mech. **46**, 199 (1971)
19. S. Spagnolie, E. Lauga, J. Fluid Mech. **700**, 105 (2012)
20. H. Masoud, H.A. Stone, M.J. Shelley, J. Fluid Mech. **733**, (2013)
21. S. Palagi, E.W.H. Jager, B. Mazzolai, L. Beccai, Bioinspir. Biomim. **8**, 046004 (2013)
22. A. Vilfan, Phys. Rev. Lett. **109**, 128105 (2012)
23. L. Zhu, E. Lauga, L. Brandt, J. Fluid Mech. **726**, 285 (2013)
24. P. Underhill, M.D. Graham, Phys. Fluids **23**, 121902 (2011)
25. Carolina Protozoa, and Invertebrates Manual. Burlington, North Carolina: Carolina Biological Supply Company (2010)
26. A. Eckstein, J. Charonko, P. Vlachos, Exp. Fluids **45**, 485 (2008)
27. A. Eckstein, P.P. Vlachos, Meas. Sci. Technol. **20**, 055401 (2009)
28. A. Eckstein, P.P Vlachos, Meas. Sci. Technol. **20**, 075402 (2009)
29. F. Scarano, M. L. Riethmuller, Exper. Fluids **26**, 513 (1999)
30. R. Hain, C.J. Kähler, Exper. Fluids **42**, 575 (2007)
31. C. Pozrikidis, *Boundary Integral and Singularity Methods for Linearized Viscous Flow* (Cambridge University Press, 1992)
32. C. Pozrikidis, *A Practical Guide to Boundary Element Methods with the Software Library BEMLIB* (CRC Press, 2002)
33. L. Zhu, E. Lauga, L. Brandt, Phys. Fluids **24**, 051902 (2012)
34. I. Jung, T.R. Powers, J.M. Valles Jr., Biophys. J. **106**, 106 (2014)